Physics-based modeling of AlGaAs tunnel junction VCSELs: a comparative appraisal

Alberto Gullino[†*], Valerio Torrelli[*†], Martino D'Alessandro[*†], Alberto Tibaldi[*†],
Francesco Bertazzi[*†], Michele Goano[*†], and Pierluigi Debernardi[†]
[*] Dipartimento di Elettronica e Telecomunicazioni, Politecnico di Torino, Corso Duca degli Abruzzi 24, 10129 Torino, Italy
[†] CNR-IEIIT, Corso Duca degli Abruzzi 24, 10129 Torino, Italy
E-mail: alberto.gullino@polito.it

***Abstract*—In this paper, we adopt our in-house physics-based solver VENUS (Vcsel Electro-optho-thermal NUmerical Simulator) to assess the static output characteristics of an AlGaAs/GaAs TJ-VCSEL emitting at 850 nm. To this aim, VENUS is extended to exploit a combined drift-diffusion model and NEGF formalism, that accurately captures tunneling effects across the TJ. The results are compared to a commercial *pin*-like VCSEL, at temperatures ranging from 20 to 110°C, to cover a broad set of operations from room temperature to harsh environments.**

I. Introduction

Commercial vertical-cavity surface-emitting lasers (VCSELs) for short-distance communication purposes emitting in the 850–980 nm window are mostly based on AlGaAs/GaAs VCSELs [1]. These are *pin*-like devices, where the intrinsic GaAs-based active region (AR) is sandwiched between oppositely doped distributed Bragg's reflectors (DBRs). An oxide aperture realized through wet oxidation of Al-rich layers is grown in the proximity of the AR to ensure both optical and electrical confinement.

At other wavelengths, similar concepts are replicated taking advantage of the introduction of buried tunnel junctions (TJs). TJs are efficient hole injectors, as they are reversely-biased heavily doped *pn* junctions where carrier transport occurs through band-to-band tunneling (BTBT). In addition, they are realized through controllable etching steps, allowing a precise definition of the active volume without oxide apertures. This boosted the development of InP-based and GaSb-based TJ-VCSELs emitting respectively at 1.3–2.6 μm and 2.3–3, 4 μm, where the realization of oxides can be critical. Furthermore, in nitride-based TJ-VCSELs for UV emission the *p*-doped DBRs are replaced by *n*-doped layers, addressing the issue related to the huge acceptor ionization energies that prevent an efficient hole transport across the *p*-DBR.

Nevertheless, TJs hold the promise of a revolution in AlGaAs VCSELs as well, due to the possibility to mitigate the overall device resistivity, paving the way towards higher speeds and lower losses. In this paper, we investigate the effectiveness of introducing TJs in AlGaAs VCSELs. In this first example of application of our comprehensive solver, the TJ is used to avoid the highly resistive and absorbing top *p*-DBR, with the confinement still on charge of an oxide aperture. To demonstrate the benefits of a TJ-VCSEL, we compare it to an equivalent *pin* device. The extremely rapid

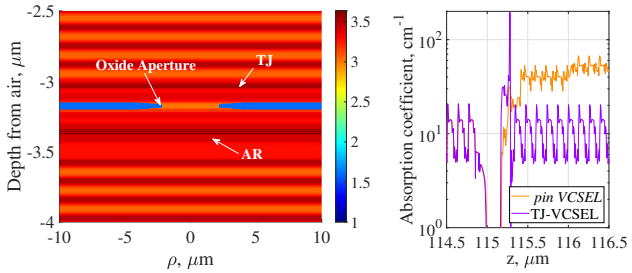

(a) (b)

Fig. 1: Refractive index of the TJ-VCSEL (**a**) and absorption profiles in the proximity of the AR (**b**).

VCSEL market evolution suggests that a minimization of on-wafer prototypes is highly preferable. Therefore, we propose a technologically computer aided design (TCAD) approach by exploiting our in-house electro-opto-thermal VCSEL simulator VENUS [2], [3], self-consistently coupled to a nonequilibrium Green's function (NEGF) formalism describing rigorously the BTBT in the TJ region [4], [5].

II. Results and Outlooks

VENUS has been developed by our group to investigate a commercial *pin* VCSEL [2], [3]. Here, we use it as a reference device, to be compared with a TJ-VCSEL obtained modifying the minimum number of layers possible. The two devices under study feature a 1λ-cavity embedding three 8 nm GaAs quantum wells (QWs). The bottom *n*-DBR is made of 36 pairs with alternating Al molar concentration. The top DBRs are designed to achieve similar optical threshold gains in the two VCSELs. Therefore, the 21 pairs (*p*-doped) of the *pin* device are reduced to 19 (*n*-doped) in the TJ-VCSEL, taking advantage of the lower free-carrier absorption (FCA) losses in the *n*-doped mirror in the latter device [5], [6].

The TJ is exploited here only as hole injector, while confinement still relies on an oxide aperture with diameter of 4.75 μm and thickness of 30 nm as in the *pin* VCSEL. This is the only chance to minimize the differences between a *pin* and TJ-VCSEL and to perform a close comparison between the two injections techniques. In fact, structuring the TJ by selective etching and regrowing on it the top DBR would completely change the guiding features of the VCSEL. In this device, the TJ extends across the whole mesa, meaning that no further technological steps are introduced with respect to

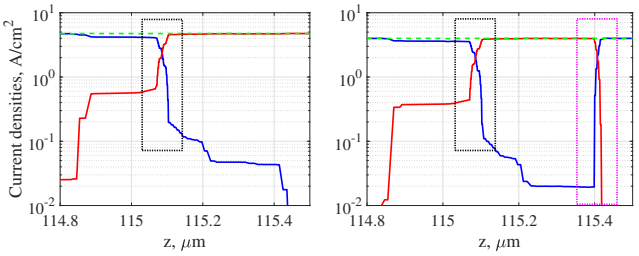

(a) *pin*-VCSEL (b) TJ-VCSEL

Fig. 2: Electron (blue) and holes (red) current densities at 5 mA, and their sum (green), for (**a**) *pin* and (**b**) TJ-VCSEL. The dotted boxes are used to indicate the QWs (black) and TJ (purple) regions.

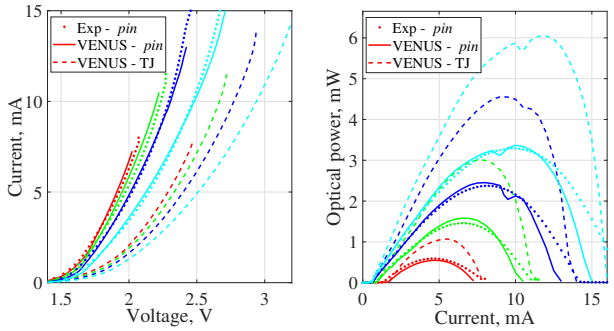

(a) *IV* (b) *LI*

Fig. 3: (**a**) Electrical (*IV*) and (**b**) optical (*LI*) characteristics of the two VCSELs at 20 (cyan), 50 (blue), 80 (green) and 110°C (red). Experimental data and VENUS results on the *pin* device are reported as dots and solid lines, respectively; VENUS results on the TJ-VCSEL are shown as dashed curves.

conventional VCSEL growth. This can be seen in the zoom of the refractive index profile of the TJ-VCSEL provided in Fig. 1a. The alternating layers of the DBRs are represented in shades of orange and red. The radially graded oxide aperture is surrounded by the oxidized region (light blue); three dark stripes in the AR denote the QWs; the TJ has an Al molar fraction close to the DBR, and is indicated in the figure.

Positioning the TJ requires particular attention. Its high doping introduces strong FCA losses in the TJ, reflecting into the high absorption coefficient reported in Fig. 1b. When moving to TJ-VCSEL (purple) from a standard design (yellow), absorption remains equal in the bottom DBR, while it significantly reduces in the top *n*-DBR [3, eq. (7)]. A strong peak arises in the TJ region. To mitigate it, the TJ should be placed in a node of the optical standing wave (SW). However, a similar position is occupied by the oxide aperture to guarantee weak transverse guiding (single or few mode emission), leading to higher threshold currents [7]. In our TJ-VCSEL design, we choose to keep the oxide closer to the AR, while the TJ is grown in the next SW node.

In a standard VCSEL the electrical, optical and thermal problems are strictly connected. VENUS deals with them in a comprehensive self-consistent way, within a physics-based framework. A quantum-correct drift-diffusion model (QCDD) deals with the electrical transport problem. The optical modes of the VCSEL are computed by our in-house electromagnetic solver VELM, by imposing the resonance condition after a full round-trip, including also thermal and gain profiles. The static heat equation is solved accounting for every self-heating process. Further details about VENUS are discussed in [2], [3].

The purely quantum mechanical nature of BTBT imposes a genuine quantum approach, beyond the semiclassical DD. The novelty of this work is the introduction of the NEGF-DD framework in VENUS, as already done in its one-dimensional counterpart, D1ANA [4], [5], [6]. Following the same approach, self-consistency between the QCDD solver and NEGF formalism is achieved by extracting from the latter a generation rate accounting for the BTBT inside the TJ, which depends on the voltage drop across it. This rate is then introduced into the bulk layers treated with the DD model alongside other recombination rates.

In Fig. 2, the electron and hole current densities are shown along the vertical direction. Their sum is conserved, as expected and shown by the green dashed lines. In the reference device (Fig. 2a), electrons and holes reach the QWs from oppositely doped DBRs. In the QWs, the radiative recombinations cause the switch of the dominant current contributions. TJ-VCSEL (Fig. 2b) still injects electrons from the bottom DBR, but holes come from BTBT in the TJ. Since the hole current density reached in the TJ-VCSEL is identical to the *pin* VCSEL counterpart from the DBR, the TJ is working properly.

Eventually, Fig. 3 reports the static electrical (*IV*) and optical (*LI*) characteristics at different temperatures. TJ-VCSEL *IV* curves (Fig. 3a) display lower currents at equal applied bias than the reference device, at every temperature. This is related to the additional voltage drop across the TJ, that lies in the range of 0–0.8 V. Such electrical penalty is largely compensated by improvements in the *LI* curves (Fig. 3b), where the TJ-VCSEL almost doubles the maximum output optical power. Since the removal of almost all the *p*-doped layers in the TJ-VCSEL allows to remove two pairs from the top DBR, the corresponding LI slope significantly increases. This confirms the results coming from our 1D approach [5]. As imposed by the similar optical threshold gains, the threshold currents of the two VCSELs stay similar at every temperature.

Our efforts will be now devoted towards the analysis of AlGaAs VCSELs where also confinement comes from TJ. This would allow to get rid of the oxidation process that limits the aperture size accuracy, crucial to reach very small active sizes.

References

[1] R. Michalzik, ed., *VCSELs: Fundamentals, Technology and Applications of Vertical-Cavity Surface-Emitting Lasers* (Springer-Verlag, Berlin, 2013).

[2] A. Tibaldi, F. Bertazzi, M. Goano, R. Michalzik, P. Debernardi, *IEEE J. Select. Topics Quantum Electron.* **25**, 1500212 (2019).

[3] P. Debernardi, *et al.*, *IEEE J. Select. Topics Quantum Electron.* **25**, 1700914 (2019).

[4] A. Tibaldi, *et al.*, *Phys. Rev. Appl.* **14**, 024037 (2020).

[5] A. Gullino, *et al.*, *21st International Conference on Numerical Simulation of Optoelectronic Devices (NUSOD 2021)* (online, 2021), pp. 79–80.

[6] A. Gullino, A. Tibaldi, F. Bertazzi, M. Goano, P. Debernardi, *Proceedings of SIE 2022*, G. Cocorullo, F. Crupi, E. Limiti, eds. (Springer Nature Switzerland, Cham, 2023), pp. 190–195.

[7] B. Demeulenaere, P. Bienstman, B. Dhoedt, R. G. Baets, *IEEE Journal of Quantum Electronics* **35**, 358 (1999).